Clinical Ophthalmology

Dovepress
Taylor & Francis Group

Open Access Full Text Article

ORIGINAL RESEARCH

TRAP1 Improves Diabetic Retinopathy by Preserving Mitochondrial Function

Yuchen Li[1,*], Weida Xu[1,*], Guiyang Zhao[1,*], Yuchen Guo[1], Liyuan Wang[1], Qianming Du[2], Yuxiang Fei[3], Xueteng Hu[1], Haoshen Hu[1], Lixun Chen[1,4], Yidan Xu[1,4]

[1]Department of Ophthalmology, Nanjing First Hospital, Nanjing Medical University, Nanjing, People's Republic of China; [2]General Clinical Research Center, Nanjing First Hospital, Nanjing Medical University, Nanjing, People's Republic of China; [3]Department of Pharmacy, Nanjing First Hospital, Nanjing Medical University, Nanjing, People's Republic of China; [4]Nanjing Red Cross Eye Bank, Nanjing, People's Republic of China

*These authors contributed equally to this work

Correspondence: Lixun Chen; Yidan Xu, Department of Ophthalmology, Nanjing First Hospital, Nanjing Medical University, Nanjing, People's Republic of China, Email lixunchen@hotmail.com; yidanxu7771@gmail.com

Background: Recent studies have demonstrated that mitochondrial dysfunction is pivotal in early diabetic retinopathy (DR). Tumor necrosis factor-associated protein 1 (TRAP1), a mitochondrial chaperone regulating stress responses, remains unexplored in DR pathogenesis.

Methods: We established in vivo and in vitro models of DR. Hematoxylin and eosin (H&E) staining was utilized to evaluate retinal lesions in rats. Western blotting, reverse transcription quantitative polymerase chain reaction (RT-qPCR), and immunofluorescence staining were employed to assess TRAP1 expression in the retina. Cell viability, reactive oxygen species (ROS), mitochondrial damage, and TRAP1 expression levels were measured in ARPE-19 cells. RNA sequencing (RNA-seq) identified gene expression and pathway changes in shTRAP1 cells. The role of TRAP1 in ferroptosis in ARPE-19 cells was evaluated with or without ferrostatin-1 (Fer-1) and erastin. Potential ferroptosis-related proteins interacting with TRAP1 were validated using co-immunoprecipitation (CO-IP) techniques. This study confirmed TRAP1's critical role in the pathogenesis of DR.

Results: Our findings elucidate a significant reduction in TRAP1 expression in diabetic rat retinas, particularly in the pigment epithelium. High glucose levels correspondingly diminished TRAP1 expression in ARPE-19 cells, causing decreased cellular viability, increased ROS generation, and mitochondrial dysfunction. Notably, the overexpression of TRAP1 effectively preserved mitochondrial homeostasis under stress, mitigated mitochondrial impairment, and enhanced cellular viability. Importantly, TRAP1 may alleviate hyperglycemia-induced mitochondrial damage by reducing ferroptosis through its interactions with ferroptosis-related proteins, including acyl-CoA synthetase long-chain family member 1 (ACSL1), acyl-CoA synthetase long-chain family member 4 (ACSL4), and cytochrome b5 reductase 1 (CYB5R1).

Conclusion: TRAP1 exerts a protective influence on mitochondrial function in ARPE-19 cells. Reduced levels of TRAP1 may play a crucial role as an early contributor to mitochondrial dysfunction in diabetic retinopathy. Furthermore, the association of TRAP1 with ferroptosis improves cellular viability by enhancing mitochondrial resilience against high glucose-induced stressors and preventing cellular ferroptosis.

Keywords: diabetic retinopathy, TRAP1, mitochondria, oxidative stress, ferroptosis

Background

Diabetic retinopathy (DR) is a prevalent and distinct microvascular complication of diabetes, affecting approximately one-third of diabetic patients and serving as a primary cause of vision loss among elderly individuals with diabetes.[1] Global projections indicate that by 2030, DR will affect an estimated 127 million people. The predominant pathological changes in DR involve damage to retinal microvascular cells, leading to microvascular circulatory disorders, localized tissue ischemia, hypoxia, disruption of the blood-retinal barrier, and ultimately, neovascularization.[2] The pathogenesis of DR is primarily characterized by oxidative stress, an inflammatory response, and excessive activation of the renin-

Received: 9 February 2025
Accepted: 4 July 2025
Published: 16 July 2025

angiotensin system. The prevailing theory suggests that elevated blood glucose levels exacerbate tissue oxidative stress, resulting in damage to retinal microvessels.[3]

Mitochondria, serving as the hub for cellular respiration and metabolism, primarily produce adenosine triphosphate (ATP) to regulate cellular metabolism and apoptosis. Given their crucial role, mitochondrial dysfunction profoundly disrupts tissue homeostasis.[4] Early-stage diabetes manifests as bioenergetic alterations in various cell types, particularly in the retina, where these changes contribute to oxidative stress, mitochondrial dysfunction, and early visual impairments. Concurrently, mitochondrial dysfunction disrupts the redox state, intensifying oxidative stress. Consequently, mitochondrial dysfunction in the early stages of diabetic retinopathy may precede observable neurodegenerative changes and microvascular diseases.[5]

Recently, ferroptosis has emerged as an iron-dependent, lipid peroxidation-driven form of programmed cell death.[6] Ferroptosis is triggered when the accumulation of lipid reactive oxygen species (ROS) surpasses the oxidative-reductive equilibrium maintained by glutathione (GSH) and phospholipid hydroperoxide peroxidase, which utilizes GSH as a substrate.[7] Increasing evidence underscores the significant involvement of mitochondria in cellular ferroptosis.[8]

TRAP1, a subtype of the heat shock protein 90 (HSP90) family, functions as a molecular chaperone located on the inner mitochondrial membrane. It facilitates the folding of mitochondrial target proteins, ensuring their stability and maturation.[9] Its substrates encompass various signaling molecules, including kinases and transcription factors, thereby playing a crucial role in cell growth and development.[10] Research indicates that TRAP1 exerts significant physiological functions, participating in the regulation of mitochondrial energy metabolism and assuming a critical role in mitochondrial protein quality control.[11] Notably, TRAP1 modulates oxidative phosphorylation (OXPHOS). Through its interactions with the mitochondrial electron transport chain, TRAP1 promotes glycolysis.[12] By inhibiting complexes II and IV, TRAP1 leads to OXPHOS downregulation and reduced ROS production, which shifts the metabolic equilibrium towards aerobic glycolysis, thereby fostering NADPH generation and further diminishing ROS levels.[13]

Studies have shown that in TRAP1 knockout (TRAP1-/-) mice, mouse embryonic fibroblasts (MEFs) exhibit impaired mitochondrial function compared to wild-type (WT) controls, characterized by a marked increase in reactive oxygen species (ROS) production and heightened susceptibility to oxidative damage.[14] The mitochondrial permeability transition pore (mPTP) plays a critical role in maintaining mitochondrial homeostasis.[15] Opening of the mPTP triggers the loss of mitochondrial membrane potential ($\Delta\psi m$), rupture of the mitochondrial membrane, release of cytochrome C (CytC) into the cytosol, and subsequent induction of apoptosis.[16] Cyclophilin D (CypD), a mitochondrial matrix protein, serves as a key regulator of mPTP activity.[17] Liu et al further demonstrated that TRAP1 overexpression inhibits mPTP opening through direct interaction with CypD, thereby preserving mitochondrial integrity, attenuating oxidative stress and apoptosis, and ultimately improving renal function and mitigating pathological damage in diabetic rats. These findings underscore TRAP1's essential protective role in diabetic kidney disease (DKD).[18–20] However, no association between TRAP1 and diabetic retinopathy (DR) has been reported to date, and the mechanisms underlying its potential to safeguard retinal mitochondrial activity and redox homeostasis under hyperglycemic stress remain unclear.

In this study, we have substantiated the hypothesis that TRAP1 is implicated in the mechanisms of mitochondrial injury in early DR. Our findings provide evidence for TRAP1's potential role in ameliorating diabetes-associated retinal lesions by preserving mitochondrial function and cellular activity. Comprehensive investigations reveal TRAP1's involvement in cellular ferroptosis, and inhibiting mitochondrial ferroptosis under high glucose stress conditions may represent an important pathway for preserving cellular function. These discoveries enhance our understanding of the mechanisms underlying early-stage mitochondrial dysfunction in DR, laying the foundation for further research into protective measures against early DR and potential gene-targeted therapies in the future.

Methods and Materials

Reagents and Antibody

The following reagents are commercially available: Streptozotocin (S8050) from Solarbio (Beijing, China), D-Glucose Anhydrous (1179GR500) from BioFroxx (Germany), Erastin (S7242), Ferrostatin-1 (S7243), Z-VAD-FMK (S7023), 3-Methyladenine (S2767), and Necrostatin-1 (S8037) from Selleck Chemicals (Houston, USA), Puromycin (ST551) from

Beyotime (Shanghai, China), and a pre-stained protein marker (26617) from Thermo Fisher (Waltham, USA). Additionally, TRAP1 Polyclonal antibody (10325-1-AP), Beta Actin Polyclonal antibody (20536-1-AP), COXIV Polyclonal antibody (11242-1-AP), Tom20 Polyclonal antibody (11802-1-AP), HRP-conjugated Goat Anti-Rabbit IgG (H+L) (SA00001-2), CoraLite594-conjugated Goat Anti-Rabbit IgG(H+L) (SA00013-4), and CoraLite488-conjugated Goat Anti-Mouse IgG(H+L) (SA00013-1) are sourced from Proteintech (Wuhan, China).

Experimental Animals

All experimental animals were male Sprague-Dawley (SD) rats, aged 8 weeks, with a weight range of 290 to 350 g and an average weight of 320 g. These rats were procured from the Zhejiang University School of Medicine (Hangzhou, China; SCXK (Zhe) 2019–0002). The animals were housed in the SPF-level Animal Experimental Center at the First Affiliated Hospital of Nanjing Medical University (Nanjing, China; SCXK (Su) 2021–0007). They were maintained under standardized conditions at a temperature of (20±3) °C, with humidity ranging from 50% to 60%, and a 12-hour light-dark cycle for one week to facilitate acclimatization. The rats were provided with standard rodent chow and had unrestricted access to water and food. Ethical approval for this study was obtained from the Ethics Committee of the First Affiliated Hospital of Nanjing Medical University, with the ethics number DWSY-22165292. The research strictly adhered to the principles outlined in the "Laboratory Animals" publication by the National Institutes of Health (NIH Publications No. 80–23). All animals were treated humanely, and rigorous efforts were made to minimize potential discomfort or pain experienced by the animals.

In this study, SD rats were randomly allocated into four groups: control, 4-week, 8-week, and 12-week groups. After a one-week acclimatization period, the experimental groups transitioned gradually to a high-fat diet consisting of 45% fat for two weeks (purchased from Synergistic Biologics, Nanjing, China; XTHF45-1). Following a 12-hour fasting period with free access to water, the experimental group received an intraperitoneal injection of streptozotocin (STZ) at a dosage of 35 mg/kg, while the control group received an intraperitoneal injection of physiological saline.[20,21] Tail vein blood samples were collected 72 hours post-injection to measure fasting blood glucose. High-fat feeding continued for an additional four weeks, after which fluorescence angiography was performed.

Hematoxylin and Eosin (HE) Staining

Retinas from both eyes of rats were obtained and subjected to a series of preparatory steps, including freezing in liquid nitrogen, routine dehydration, transparency treatment, and paraffin embedding, to produce 5 μm sections. Following the drying of the sections, deparaffinization was performed, and the samples were rehydrated in varying concentrations of alcohol for 5 minutes each. Hematoxylin staining was conducted using hematoxylin (Beyotime; C0105S) for 15 minutes, followed by three washes with PBS. Differentiation was subsequently achieved by treating the sections with hydrochloric acid alcohol for 30 seconds, followed by thorough washing and staining with 1% eosin. After alcohol dehydration, the deparaffinization process was completed, and the slides were examined under a microscope after sealing.

Cell Culture

ARPE-19 cells were obtained from Procell (Wuhan, China; CL-0026) and maintained at 37°C in a 5% CO_2 atmosphere using Dulbecco's Modified Eagle Medium/Nutrient Mixture F-12 (1:1), supplemented with 10% fetal bovine serum (FBS) (Procell; 164210) and KeyGEN Biotech (Nanjing, China; KGM12500-500). Co-cultivation of ARPE-19 cells was conducted with glucose concentrations of 25, 33, 40, 50, and 100 mM for durations ranging from 1 to 6 days, designating the cells treated with 50 mM glucose for 6 days as the high glucose (HG) group. The cells used in this study were within the third to seventh passage following recovery.

Construction of Overexpression and Knockdown Cell Lines

TRAP1 overexpression, TRAP1 knockdown, and lentiviruses containing a control vector were obtained from Genechem (Shanghai, China). ARPE-19 cells were cultured in 6-well plates until they reached 30% confluence. Subsequently, the culture medium was replaced with 1 mL of lentivirus-containing medium and 40 μL of HiTransG P. The cells were then incubated for 16 hours at a multiplicity of infection (MOI) of 10. Following this, the medium was replaced with DMEM/

F12 medium supplemented with only fetal bovine serum (FBS), and the cells were cultured for an additional 72 hours. HiTransG P was utilized to enhance infection efficiency. Finally, the cells were cultured in complete medium containing puromycin (1 μg/mL) for 48 hours prior to subsequent experiments.

RNA Extraction, cDNA Synthesis, and Quantitative Reverse Transcription Polymerase Chain Reaction (qRT-PCR)

Total RNA was extracted from cells, retina, and choroid tissue using the RNA isolater Total RNA Extraction Reagent (Vazyme; Nanjing, China; R401-01). The extracted RNA was dissolved in DEPC water (KeyGEN Biotech; KGDN4100), and its purity and concentration were assessed using a spectrophotometer. Subsequently, 1 μg of total RNA from each sample was reverse transcribed into complementary DNA (cDNA) utilizing the HiScript III All-in-one RT SuperMix Perfect for qPCR Kit (Vazyme; R333). For quantitative real-time polymerase chain reaction (qRT-PCR), 10 μL of 2x Taq Pro Universal SYBR qPCR Master Mix (Vazyme; Q712) was employed. The PCR conditions included pre-denaturation at 95°C for 30 seconds, followed by denaturation at 95°C for 10 seconds, and annealing at 60°C for 30 seconds, totaling 40 cycles of standard PCR. A melting curve was generated at 95°C for 15 seconds, 60°C for 60 seconds, and 95°C for 15 seconds. Quantification of gene expression was performed using the 2-ΔΔCt method, with expression values normalized to Beta Actin mRNA, which exhibited stable levels across all samples. The experiment was conducted in triplicate.

The primer sequences for real-time fluorescence quantitative PCR were as follows:

TRAP1 (human): forward 5'-CGCAGCATCTTCTACGTGC-3',
reverse 5'-CTGATGAGTGCGCTCTCC-3'

TRAP1 (rat): forward 5'-CTCAGTTGCTACAGCCCACA-3',
reverse 5'-CTGCTATCATGGCGTTCTCA-3'

Beta-Actin(human): forward - CACACGGAGTACTTGCGC-3'
reverse 5'- TCAGGTCATCACTATCGGCAAT-3',

Beta-Actin(rat): forward 5'5'-CGCAAAGACCTGTACGC-3',
reverse 5'- AAAGAAAGGGTGTAAAACGCA-3'.

Western Blotting

Proteins were extracted from cells, retina, and choroid tissue using RIPA lysis buffer (NCM Biotech; Suzhou, China; WB3100), which contained proteinase and phosphatase inhibitors (KeyGEN Biotech; KGP603, KGP602). The protein concentration was determined with the BCA Protein Assay Kit (KeyGEN Biotech; KGP902). Protein samples were separated using a 10% ExpressCast PAGE Colored Gel Rapid Kit (NCM Biotech; P2012) in electrophoresis buffer and subsequently transferred to a PVDF membrane using Rapid Transfer Buffer (NCM Biotech; WB4600). After blocking with 5% skimmed milk for 1 hour, the membrane was incubated with primary antibodies overnight at 4°C. Following this, the membrane was incubated with secondary antibodies at room temperature for 1 hour. Finally, Enhanced Chemiluminescent (ECL) detection (NCM Biotech; P2300) was utilized for fluorescence imaging. Quantification was performed using ImageJ software, and the experiment was repeated at least three times.

Cellular Viability Assessment

Cellular viability was assessed using the CCK-8 Cell Proliferation Assay Kit (KeyGEN Biotech; KGA317). ARPE-19 cells were seeded in a 96-well plate and cultured in serum-free medium for 24 hours. Following this, various interventions were performed, and cellular viability was evaluated at designated time points. To each well containing 1 × 10^4 cells, 10 μL of CCK-8 detection solution was added. After incubation at 37°C for 1 hour, the absorbance of each well was measured at a wavelength of 450 nm using a microplate reader. The experiment was independently repeated three times.

Measurement of ROS Generation

The intracellular reactive oxygen species (ROS) levels were assessed using the 2',7'-Dichlorodihydrofluorescein diacetate (DCFH-DA) staining method (KeyGEN Biotech; KGT010-1). Following treatment with 50 mM high glucose for 1–6 days, ARPE-19 cells were collected and incubated in serum-free medium containing DCFH-DA (10 μM) at 37°C for 20 minutes, with gentle inversion and mixing every 5 minutes. Subsequently, the cells were washed three times with serum-free medium and resuspended in phosphate-buffered saline (PBS). The ROS levels were quantified using a flow cytometer with 488 nm laser excitation and fluorescence signal detection in the 530/30 nm channel. All procedures were performed under light-protected conditions. Data analysis was conducted using FlowJo 10.8.1 software (Tree Star Inc.; Ashland, USA) to quantify ROS levels based on mean fluorescence intensity (MFI). Three independent experiments were performed to ensure reliability.

Immunofluorescence

Paraffin sections of rat eyeballs were deparaffinized after being baked at 60°C for 2 hours. Antigen retrieval was performed using 20×Tris-EDTA Antigen Retrieval Solution (pH9.0) (Servicebio; Wuhan, China; G1203). Following permeabilization with TritonX-100 (Beyotime; P0096) for 10 minutes, blocking was carried out with 10% goat serum (Solarbio; SL038) at room temperature for 1 hour. After triple rinsing with PBS, sections were incubated with primary antibodies overnight at 4°C. On the subsequent day, samples were incubated with secondary antibodies for 1 hour.

ARPE-19 cells were seeded in a 24-well plate with cover slips and washed twice with PBS at the respective time points. Cells were fixed for 15 minutes using universal tissue fixative (Servicebio; G1101) and washed thrice with PBS. Following permeabilization with TritonX-100 for 10 minutes, cells were blocked with 10% goat serum at room temperature for 30 minutes. Subsequently, cells were co-incubated with anti-TRAP1 and anti-Tom20 primary antibodies overnight at 4°C. On the subsequent day, samples were co-incubated with CoraLite488 and CoraLite594 secondary antibodies for 1 hour. After triple washing with PBS, cover slips were mounted on glass slides using anti-fade mounting medium (containing DAPI) (Beyotime; P0131) and incubated in the dark for 10 minutes.

Images were acquired using AxioImager M2 (Zeiss), and analysis was executed using Zen3.1 software (Zeiss, Rueil Malmaison, France). Quantitative analysis was performed using Image J software.

Detection of Mitochondrial Membrane Potential ($\Delta\psi m$)

Mitochondrial membrane potential ($\Delta\Psi m$) was assessed using the JC-1 Assay Kit (KeyGEN Biotech; KGA603-1). ARPE-19 cells seeded in 24-well plates were subjected to experimental conditions or treated with 10 μM CCCP for 20 minutes as a positive control. Subsequently, cells were incubated with 2 μM of the JC-1 working solution at 37°C for 20 minutes in the dark. After incubation, the cells were washed twice with Incubation Buffer and imaged using a Zeiss AxioImager M2 microscope equipped with dual-wavelength settings: JC-1 aggregates (indicative of intact $\Delta\Psi m$, red fluorescence: Ex 488 nm/Em 590–650 nm) and monomers (indicative of depolarized $\Delta\Psi m$, green fluorescence: Ex 488 nm/Em 500–550 nm). To prevent spectral overlap, sequential channel acquisition was employed. Images were analyzed using Zen 3.1 software, and the ratios of aggregates to monomers fluorescence were quantified via ImageJ to normalize probe-loading variability. Three independent experiments were conducted, each with triplicate wells, including both unstained and CCCP-treated controls.

Detection of Mitochondrial Permeability Transition Pore (mPTP)

MPTP detection was performed using the Mitochondrial Permeability Transition Pore Assay Kit (Beyotime; C2009S). ARPE-19 cells were seeded in a 24-well plate with cover slips and washed with PBS at the respective time points. Calcein AM staining solution (1X), fluorescence quenching working solution (1X), or Ionomycin control (1X) was added to each well with a volume of 250μL.

After incubation at 37°C in the dark for 45 minutes, the medium was replaced with preheated culture medium at 37°C, and cells were incubated again in the dark for an additional 30 minutes. Cells were washed twice with PBS, images were captured using AxioImager M2, and analysis was performed using Zen3.1 software. Quantitative analysis was carried out using Image J software. The experiment was independently conducted three times.

RNA-Seq and Analysis

cDNA libraries were constructed and sequenced using RNA-seq technology at Annoroad Gene Technology Co., Ltd. (Beijing, China). Sample purity was assessed using the NanoPhotometer® spectrophotometer (Thermo Fisher), while the integrity and concentration of RNA samples were determined using the Agilent 2100 RNA Nano 6000 Assay Kit (Agilent Technologies, CA, USA). Sequencing of cDNA libraries from NC cells under high glucose stimulation and TRAP1 knockdown cells for three experimental groups was performed on the MGI platform. After filtering out sequences containing adapter sequences and low-quality sequences, high-quality Clean Reads were obtained. StringTie was employed for calculating the number of reads mapped to each gene. Gene expression was computed and expressed as Fragments Per Kilobase Million (FPKM), representing the number of fragments per thousand bases of transcript per million mapped reads. DEGSeq was utilized for identifying differentially expressed genes. The criteria for differential gene selection were as follows: fold change greater than or equal to 2, p-value less than 0.05, and q-value less than 0.05.

Transmission Electron Microscopy (TEM)

1. Cell Fixation

   Collected cells (1×10^7) were washed once with PBS, centrifuged (4°C, 2000 rpm, 5 min), and fixed overnight at 4°C with 2.5% glutaraldehyde/2% paraformaldehyde (Servicebio, G1102).

   After PBS rinsing, samples were post-fixed with 1% osmium tetroxide (OsO_4) in PBS (4°C, 1 h).
2. Dehydration & Embedding

   Fixed cells were dehydrated through an ethanol series (50%, 70%, 80%, 90%, 100%, 15 min each), transitioned to acetone, and infiltrated with Spurr's epoxy resin via graded resin/acetone mixtures.Resin-penetrated samples were cured at 60°C for 48 h.
3. Sectioning & Staining

   Ultrathin sections (70 nm) were cut using a Leica UC-7 ultramicrotome (diamond knife), stained with 2% uranyl acetate (15 min) and Reynolds' lead citrate (5 min).
4. Imaging

   Sections were imaged using a JEOL JEM-1400 TEM (80 kV) with a Gatan Orius SC1000 CCD camera. Three independent replicates were analyzed.

Malondialdehyde (MDA) Assay

The detection was conducted utilizing the Lipid Peroxidation MDA Assay Kit (Beyotime; S0131S). At specified time points, cells ($2.5x10^6$) were harvested and lysed with Western and IP cell lysis buffer (NCM Biotech; P70100). The lysates underwent centrifugation at 10,000g for 10 minutes at 4°C to collect the supernatant. The MDA detection working solution was added to the supernatant, thoroughly mixed, and subjected to a 15-minute heating step in a boiling water bath. Following centrifugation at 1000g for 10 minutes at room temperature, the supernatant was transferred to a 96-well plate, and the absorbance of each well was measured at 532 nm using a spectrophotometer. The experiment was replicated at least three times.

Iron (Fe^{2+}) Assay

The detection was performed using the Ferrous Ion Assay Kit (Solarbio; BC5415). At specified time points, cells ($2.5x10^6$) were collected, and the supernatant was obtained after ice-bath sonication and subsequent centrifugation. The appropriate reagents were added according to the manufacturer's instructions. Following centrifugation at 12,000g at room temperature for 10 minutes, the supernatant was transferred to a 96-well plate, and the absorbance of each well was measured at 593nm using a spectrophotometer. The experiment was repeated at least three times.

Determination of GSH/GSSG Activity

In accordance with the manufacturer's instructions, GSH and GSSG levels in ARPE-19 cells were evaluated using the GSH and GSSG Assay Kit (Beyotime; S0053). Glutathione reductase was employed to reduce GSSG to GSH in this

experiment. GSH reacted with the chromogenic substrate 5,5'-dithiobis(2-nitrobenzoic acid) (DTNB) to produce yellow 5'-thio-2-nitrobenzoic acid (TNB) and GSSG. This reaction served as the basis for quantifying the total glutathione content in the cells. By depleting GSH in the cells using appropriate reagents, the GSSG content in the cells was determined using the same reaction. The absorbance of each sample was measured at 412nm using a spectrophotometer. The experiment was replicated at least three times.

Lipid ROS Assay

ARPE-19 cells were seeded onto coverslips in 24-well plates. Upon reaching the desired treatment stage, the culture medium was replaced with fresh medium containing the C11-BODIPY 581/591 probe (Thermo Fisher; D3861) at a concentration of 10 μM, followed by incubation in the dark for one hour. After incubation, the cells were washed twice with PBS to eliminate uninternalized probes. Fluorescence images were captured using a Zeiss AxioImager M2 fluorescence microscope (Zeiss, Germany) with the following parameters: Oxidized state (green fluorescence): Excitation wavelength of 488 nm, emission filter of 500–550 nm;- Reduced state (red fluorescence): Excitation wavelength of 581 nm, emission filter of 590–650 nm.Images were analyzed using Zen 3.1 software and quantified with ImageJ software. A total of three independent experiments were conducted.

Statistical Analysis

All data represent a minimum of three independent experiments. Statistical analysis was executed using GraphPad Prism 9.5.1 (GraphPad, San Diego, CA). Significance between two groups was determined by the Student's *t*-test, and significance among multiple groups was determined by one-way analysis of variance (ANOVA). Data are presented as mean±standard deviation (SD), with a P-value < 0.05 considered statistically significant.

Results

In the Retina of STZ-Induced Diabetic Rats, the Level of TRAP1 Decreases

To assess TRAP1 expression levels in the retina, we established a STZ-induced diabetic rat model. The results indicated that, compared to the control group, diabetic rats exhibited a significant decrease in body weight, while fasting blood glucose levels markedly increased following STZ injection (Figure 1A and B). Hematoxylin and eosin (HE) staining of paraffin-embedded eye sections demonstrated that the retinal tissue layers in the control group exhibited close packing, orderly cell arrangement, and normal morphology. However, at four weeks post-modeling, the diabetic group displayed a slightly loose retinal structure and a swollen, rough inner limiting membrane. At eight weeks post-modeling, the retinal layers became less distinct, and the cell arrangement showed increased disorder. By twelve weeks post-modeling, the retinal layers were indistinct, with significant thinning of the nerve fiber layer, inner nuclear layer, and outer nuclear layer, accompanied by disordered cell arrangement and reduced cell numbers (Figure 1C). These experimental results confirmed the successful establishment of the STZ-induced diabetic rat model. Subsequently, we assessed the expression of total TRAP1 in the retina and choroid using Western blot and RT-qPCR (Figure 1D and E). The results demonstrated a significant decrease in total TRAP1 expression in the DR group as the modeling time extended. To determine the expression of TRAP1 in each layer of the rat retina, immunofluorescence staining was conducted, revealing TRAP1 expression in cells across all retinal layers. Furthermore, with the progression of the modeling time, TRAP1 expression gradually decreased in cells of all layers, particularly in the local retinal pigment epithelium (RPE) layer (Figure 1F).

Under High Glucose Conditions, ARPE-19 Cell Mitochondrial Dysfunction Occurs, Accompanied by a Decrease in TRAP1 Levels

To gain a more profound understanding of the mechanisms underlying the initiation and progression of early DR, we subjected ARPE-19 cells to HG treatment to replicate the physiological and pathological conditions of diabetes, thereby establishing an in vitro DR model. Initially, we utilized the CCK-8 assay to evaluate the impact of various glucose concentrations on ARPE-19 cell viability. The results demonstrated that after 4 days of HG stimulation, cell viability decreased proportionally with increasing glucose concentrations (Figure 2A), reaching 68.5% in the group treated with

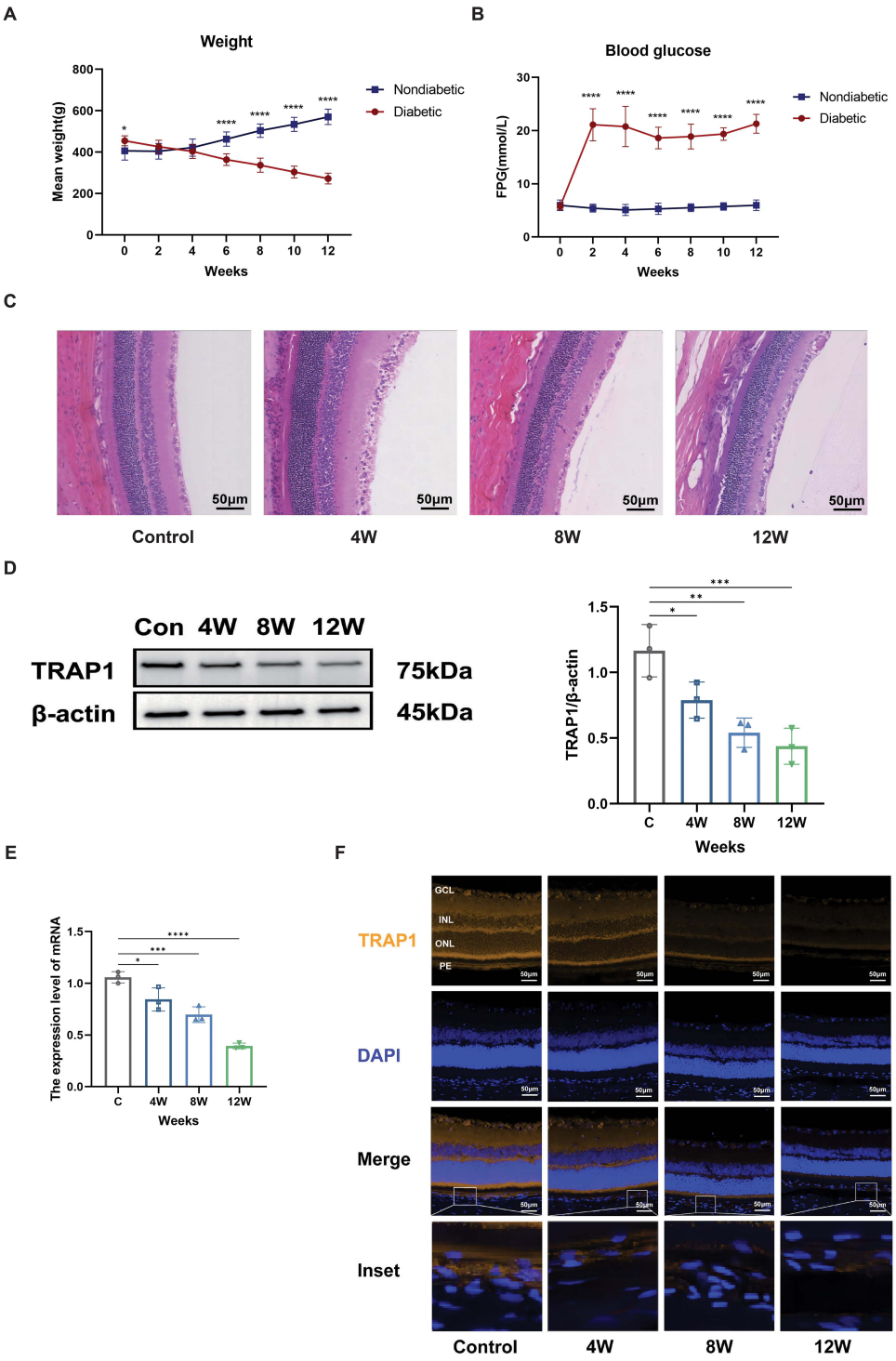

Figure 1 In the retina of STZ-induced diabetic retinopathy (DR) rat models, the level of TRAP1 decreases.**(A)** Changes in body weight during the modeling period of diabetic and control rats. (n=8) (**B**) FBG levels during the modeling period of diabetic and control rats. (n=8) (**C**) Representative micrographs of retinal sections stained with H&E from control, diabetic for 4 weeks, diabetic for 8 weeks, and diabetic for 12 weeks groups. Scale bar=50μm. (n=3) (**D**) Western blot analysis of total TRAP1 in retinal tissues from control, diabetic for 4 weeks, diabetic for 8 weeks, and diabetic for 12 weeks groups. Quantitative data are shown in the right panel. (n=3) (**E**) Total RNA was extracted from retinal tissues of control, diabetic for 4 weeks, diabetic for 8 weeks, and diabetic for 12 weeks groups, and TRAP1 mRNA expression was detected by qRT-PCR. (n=3) (**F**) Immunofluorescence staining of retinal tissue sections from each group of rats using anti-TRAP1 antibody (yellow) and DAPI (blue) for nuclear staining. The error bars in the above histograms represent the mean±SD of independent experiments.*P<0.05, **P<0.01, ***P<0.001,****P<0.0001.
Abbreviations: GCL, Ganglion cells layer; INL, Inner nuclear layer; ONL, Outer nuclear layer, PE, Pigment epithelium. Scale bar=50μm. (n=3).

50 mM glucose. Consequently, we selected 50 mM glucose for subsequent experiments and treated ARPE-19 cells for 1 to 6 days, revealing a time-dependent decline in cell viability (Figure 2B). The DCFH-DA fluorescence probe, employed through flow cytometry, facilitated the detection of intracellular ROS production (Figure 2C). The findings indicated a progressive increase in intracellular ROS levels over time, reaching nearly a four-fold increase by the sixth day. Subsequently, to explore the impact of HG on mitochondrial damage in ARPE-19 cells, we employed JC-1 and Calcein AM to assess mitochondrial membrane stability. In normal retinal cells, JC-1, depending on mitochondrial membrane potential (Δψm), rapidly enters mitochondria, exhibiting red fluorescence in a polymeric form. Conversely, when the mitochondria are damaged and Δψm decreases, JC-1 is released into the cytoplasm, displaying green fluorescence in a monomeric form. After 2, 4, and 6 days of HG treatment, Δψm in ARPE-19 cells gradually decreased with increasing exposure time (Figure 2D). In concordance with the decrease in membrane potential, the opening of the mPTP increased (Figure 2E). These results indicate that HG induces damage to Δψm, sustained opening of mPTP, and subsequent mitochondrial dysfunction. TEM was employed to examine the ultrastructure of mitochondria in ARPE-19 cells, revealing a significant increase in mitochondrial quantity in response to HG stimulation (Figure 2F).

The mitochondrial chaperone TRAP1 plays a crucial role in mitochondrial energy metabolism and maintaining mitochondrial homeostasis. After 1 to 6 days of HG stimulation in ARPE-19 cells, we examined TRAP1 expression using Western blot and RT-qPCR techniques (Figure 2G–J). The results indicated that, compared to the control group, TRAP1 expression decreased with prolonged stimulation time, demonstrating a time-dependent trend, and was significantly reduced by day 6. Given that TRAP1 exerts its biological activity within the mitochondria, specifically at the inner mitochondrial membrane, we further evaluated TRAP1 expression within the mitochondria. The findings suggested that, similar to the changes observed in total TRAP1 expression within cells, mitochondrial TRAP1 levels decreased with extended HG stimulation, also exhibiting a time-dependent trend, and were significantly reduced by day 6 (Figure 2H–K). These observations imply that HG stimulation leads to a reduction in TRAP1 protein expression within the mitochondria of ARPE-19 cells, potentially causing damage to the mitochondrial membrane potential (Δψm), sustained opening of the mitochondrial permeability transition pore (mPTP), and resulting in mitochondrial dysfunction and impaired cell viability.

TRAP1 Can Enhance Cell Resistance to High Glucose-Induced Damage by Stabilizing Mitochondria

Subsequently, we established overexpression and knockdown phenotypes to elucidate the role of TRAP1 in ARPE-19 cells under HG stimulation. ARPE-19 cells were transduced with a TRAP1-overexpressing lentivirus, and TRAP1 expression was assessed 72 hours post-infection using Western blot and RT-qPCR. The results indicated that TRAP1 protein and mRNA levels in ARPE-19 cells infected with the $TRAP1^{OE}$ lentivirus were approximately 2.5-fold and 3-fold higher, respectively, compared to control cells. Additionally, ARPE-19 cells were transduced with shTRAP1 lentivirus, and as depicted in the figures, treatment with shTRAP1 lentivirus significantly diminished TRAP1 protein expression and mRNA levels compared to the control group (Figure 3A and B). Subsequently, immunofluorescence staining was employed to evaluate TRAP1 expression within the mitochondria. Consistent with the total cellular protein, TRAP1 expression within the mitochondria was significantly elevated in $TRAP1^{OE}$ cells and reduced in shTRAP1 cells (Figure 3C). To assess the impact of TRAP1 on the growth activity of ARPE-19 cells under HG conditions, we exposed cells from each group to HG and observed that $TRAP1^{OE}$ cells exhibited significantly enhanced cell viability compared to the control group, while shTRAP1 exacerbated cell viability impairment (Figure 3D). There were no statistically significant differences in cell viability among the groups under normal glucose conditions. Furthermore, we explored the protective role of TRAP1 in mitochondria. Our observations indicated that the overexpression of TRAP1 significantly reduced intracellular ROS levels under HG stimulation, whereas TRAP1 knockdown led to a marked increase in intracellular ROS levels (Figure 3E). This suggests that TRAP1 can protect ARPE-19 cells from oxidative damage induced by HG stimulation. Following HG stimulation, we employed JC-1 to assess mitochondrial membrane potential. The results revealed that $TRAP1^{OE}$ cells exhibited an increased Δψm compared to the control group, while shTRAP1 cells demonstrated a significant loss of Δψm (Figure 3F and G). Additionally, the use of Calcein AM to evaluate the extent of mPTP opening revealed that $TRAP1^{OE}$ cells exhibited a lower degree of mPTP opening, whereas shTRAP1

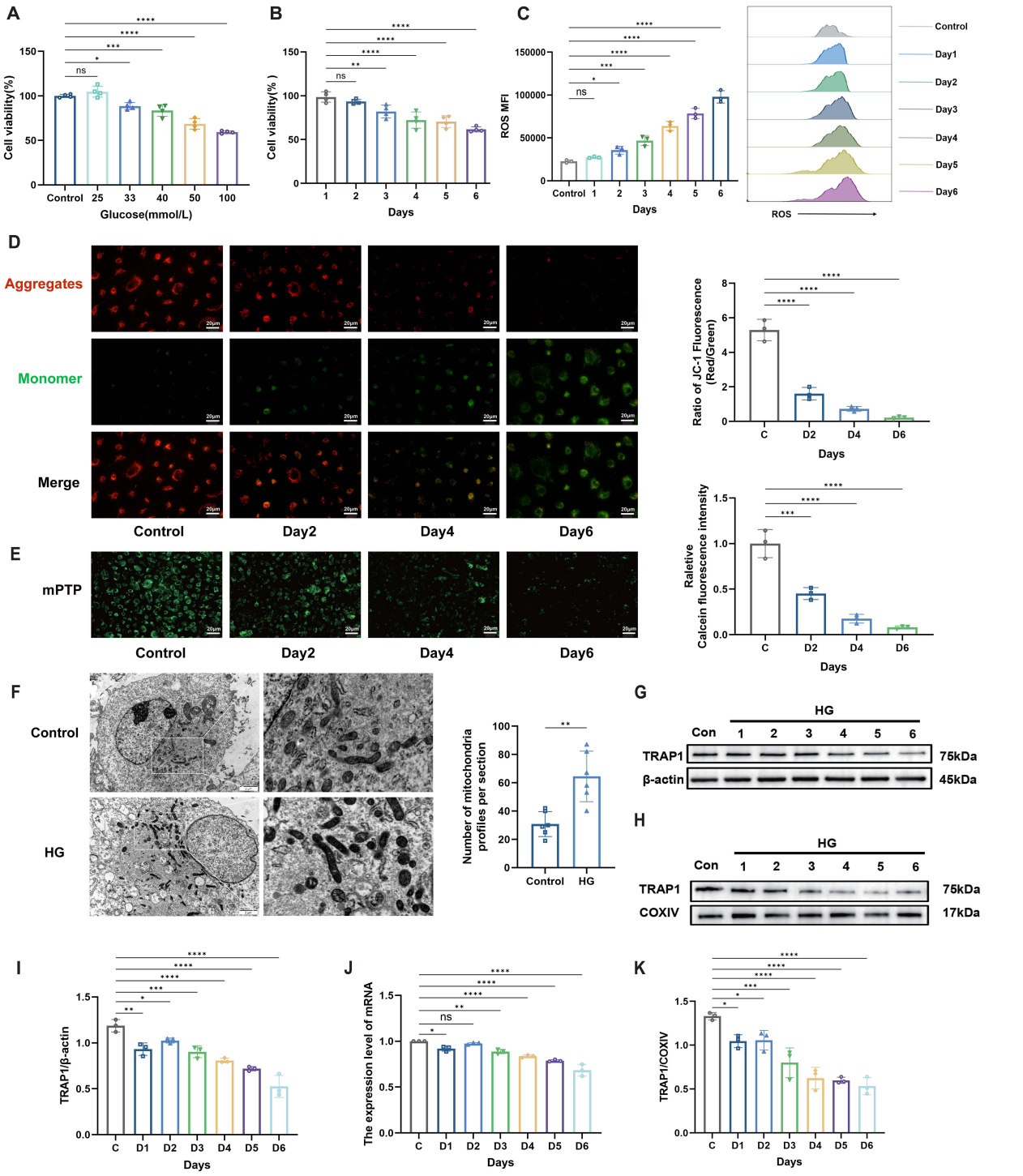

Figure 2 HG promotes mitochondrial dysfunction in ARPE-19 cells, accompanied by a decrease in TRAP1 levels. (**A**) Cell viability of ARPE-19 cells cultured with different glucose concentrations for 4 days. (n=4) (**B**) Cell viability of ARPE-19 cells cultured with 50mM glucose for 1–6 days. (n=4) (**C**) Intracellular ROS levels in cells cultured with 50mM glucose for 1–6 days. (n=3) (**D**) Identification of $\Delta\psi$ m through JC-1 staining after culturing ARPE-19 cells with 50mM glucose for 6 days. Images captured under fluorescence microscope show red fluorescence representing polymer form, indicating intact $\Delta\psi$ m, and green fluorescence representing monomer form, indicating decreased $\Delta\psi$ m. Quantified data presented on the right. Scale bar=20μm. (n=3) (**E**) ARPE-19 cells cultured with 50mM glucose for 6 days and treated with Calcein AM (1X) and CoCl2 (1X). Images captured under fluorescence microscope shown on the left. Quantified data presented on the right. Scale bar=20μm. (n=3) (**F**) TEM images of mitochondrial ultrastructure in ARPE-19 cells cultured with 50mM glucose for 6 days and control ARPE-19 cells. Quantified data presented on the right. Scale bar=2μm. (**G**) Western blot analysis of TRAP1 in ARPE-19 cells cultured with 50mM glucose for 1–6 days. (n=3) (**H**) Western blot analysis of intramitochondrial TRAP1 in ARPE-19 cells cultured with 50mM glucose for 1–6 days after mitochondrial extraction. (n=3) (**I**) Quantified data corresponding to Figure (**G**). (**J**) qRT-PCR analysis of TRAP1 mRNA expression in ARPE-19 cells cultured with 50mM glucose for 1–6 days. (n=3) (**K**) Quantified data corresponding to Figure (**H**). The error bars in the above histograms represent the mean±SD of independent experiments. ns P>0.05, *P<0.05, **P<0.01, ***P<0.001,****P<0.0001.

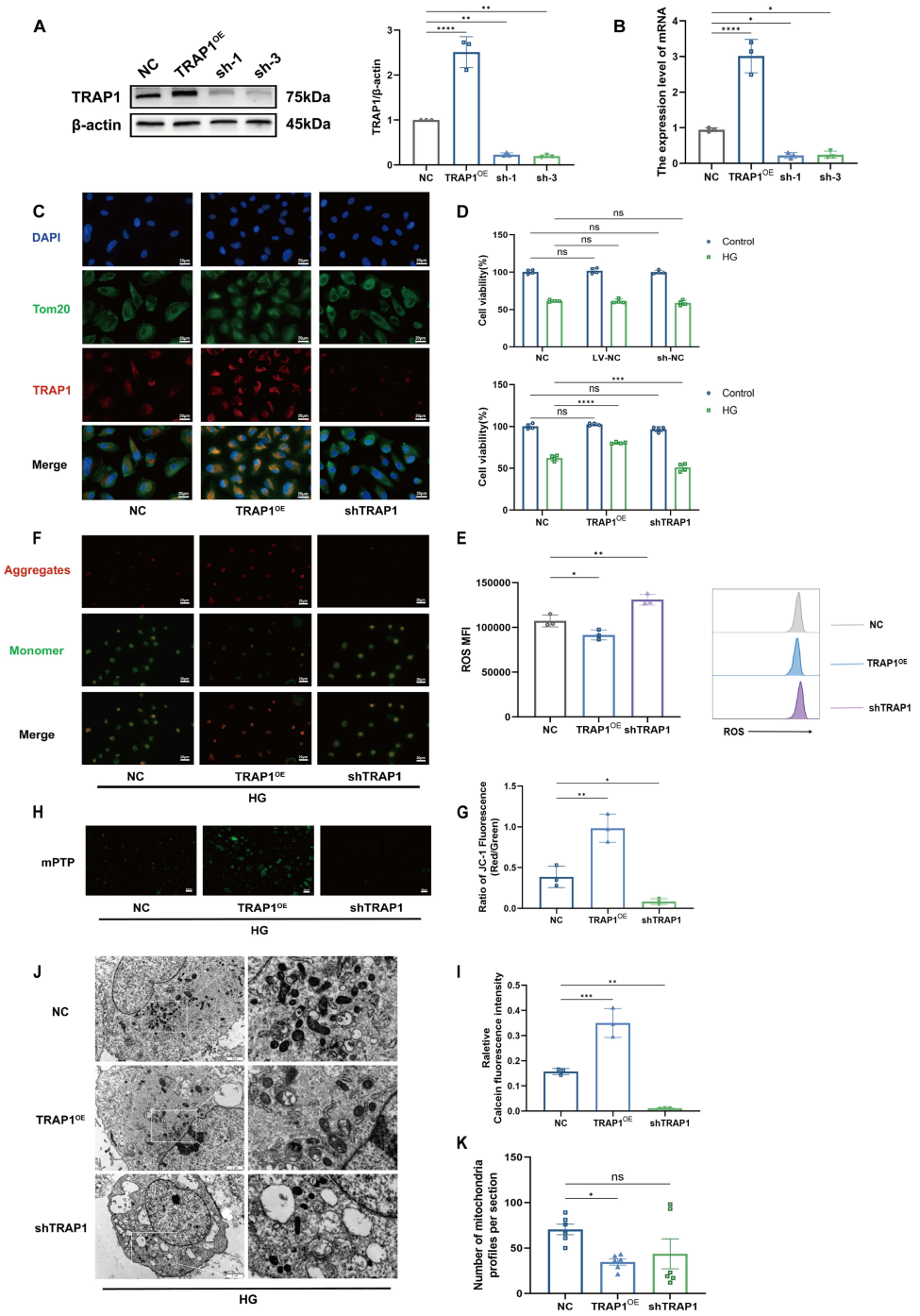

Figure 3 TRAP1 rescues mitochondrial damage under high-glucose stimulation. (**A**) The left panel depicts Western blot analysis of TRAP1 overexpression and knockdown cell lines. The right panel shows the quantified data. (n=3) (**B**) Total RNA was extracted from ARPE-19 cells overexpressing or knockdown for TRAP1, followed by qRT-PCR to assess TRAP1 mRNA expression. (n=3) (**C**) Immunofluorescence staining of TRAP1 (red) and Tom20 (green) demonstrates their colocalization in TRAP1^{OE} and shTRAP1 cells. Cell nuclei were stained with DAPI (blue). Scale bar = 20μm. (n=3) (**D**)The upper panel illustrates cell viability of NC group, cells transduced with overexpression empty virus, and cells transduced with knockdown empty virus cultured for 6 days under 50mM glucose and control conditions. The lower panel represents cell viability of NC, TRAP1^{OE}, and shTRAP1 cells cultured for 6 days under 50mM glucose and control conditions. (n=4) (**E**) Intracellular ROS levels were measured after 6 days of incubation with 50mM glucose. (n=3) (**F**) Cells cultured with 50mM glucose for 6 days were subjected to JC-1 staining to assess $\Delta\psi$ m. Fluorescence microscopy images are shown. Scale bar = 20μm. (n=3) (**G**) Quantified data from panel (**F**) are presented. (**H**) Cells cultured with 50mM glucose for 6 days were treated with Calcein AM (1X) and CoCl2 (1x). Fluorescence microscopy images are shown. Scale bar = 20μm. (n=3) (**I**) Quantified data from panel (**H**) are presented. (**J**) TEM was performed to evaluate mitochondrial ultrastructure after 6 days of incubation with 50mM glucose. Scale bar = 2μm. (**K**) Quantified data from panel (**J**) are presented. The error bars in the above histograms represent the mean±SD of independent experiments. ns P>0.05, *P<0.05, **P<0.01, ***P<0.001,****P<0.0001.

https://doi.org/10.2147/OPTH.S521660

cells displayed sustained mPTP activation (Figure 3H and I). Moreover, TEM disclosed a reduction in mitochondrial quantity in TRAP1^{OE} cells under HG stimulation (Figure 3J and K). These findings signify that TRAP1 plays a crucial role in preserving mitochondrial homeostasis under stress conditions, mitigating mitochondrial damage, and thereby safeguarding cellular function.

Knocking Down TRAP1 Affects Oxidative Stress and Related Mitochondrial Functions in ARPE-19 Cells

We conducted a comprehensive transcriptome analysis utilizing RNA-seq technology on shTRAP1 cells exposed to HG for 6 days, alongside control ARPE-19 cells. Our analysis revealed substantial differences in gene expression between the two groups, with a total of 1,260 genes exhibiting significant differential expression. Specifically, 1,006 genes were upregulated, while 254 genes were downregulated in the KD group (Figure 4A and B). Furthermore, we identified the top 50 most significantly differentially expressed genes and provided detailed information, including gene symbols, adjusted p-values, fold changes, and annotations (Supplementary Table 1).

We intersected the differentially expressed genes (DEGs) with oxidative stress-related genes (n = 1399) and risk genes associated with diabetic retinopathy (n = 716). Our analysis revealed that 131 genes overlapped between DEGs and oxidative stress-related genes, while 80 genes overlapped between DEGs and risk genes associated with diabetic retinopathy (Figure 4C). These findings suggest that TRAP1 may play a pivotal role in the onset and progression of DR by modulating oxidative stress.

Enrichment analysis of differentially expressed genes using Gene Ontology (GO) highlights a significant enrichment in essential biological processes, encompassing cell adhesion, cell migration, inflammatory response, and angiogenesis. Regarding molecular function, categories such as molecular interactions in the extracellular environment, cell signaling, structural support, and growth regulation are markedly enriched in our gene set (Figure 4D). This implies that these molecular functions may be under regulation in our experimental conditions. Regarding cellular components, the enrichment analysis predominantly highlights the mitochondrial inner membrane and extracellular matrix. Among the enriched genes are TRAP1, HMOX1, MOSPD3, TRPM8, MMP2, IDH1, and SFN. These genes play crucial roles in regulating metabolism, maintaining organelle homeostasis under stress conditions, responding to oxidative stress, inflammation, and ensuring cell protection. Additionally, they are involved in essential processes such as cell movement, tissue remodeling, angiogenesis, apoptosis, signal transduction, and the onset of tumorigenesis. This observation suggests that our set of differentially expressed genes predominantly influences mitochondrial function by actively participating in cellular metabolism and oxidative stress responses, while also affecting the degradation of the extracellular matrix, particularly within the mitochondrial inner membrane and extracellular matrix milieu.

Furthermore, employing Kyoto Encyclopedia of Genes and Genomes (KEGG) pathway enrichment analysis, we unveiled noteworthy enrichment of differentially expressed genes in the KD group within pathways, including the PI3K-Akt signaling pathway, MAPK signaling pathway, Ras signaling pathway, Rap1 signaling pathway, and AGE-RAGE signaling pathway (Figure 4E). This indicates that TRAP1 might play a pivotal role in the progression of DR through involvement in these pathways.

TRAP1 Improves HG-Induced Ferroptosis in Cells by Stabilizing Mitochondrial Activity

We employed TEM to scrutinize the ultrastructure of mitochondria in ARPE-19 cells subjected to HG stress. The findings revealed an increased mitochondrial membrane density and reduced mitochondrial cristae structure, aligning with the morphological features documented in mitochondria during ferroptosis[20] (Figure 2F). This implies the manifestation of a ferroptotic phenotype in ARPE-19 cells under HG stimulation. Additionally, we observed alterations in mitochondrial ultrastructure in TRAP1^{OE} and shTRAP1 cells under HG stimulation compared to control ARPE-19 cells. TRAP1^{OE} cells displayed diminished mitochondrial membrane density with clear mitochondrial cristae, while shTRAP1 cells

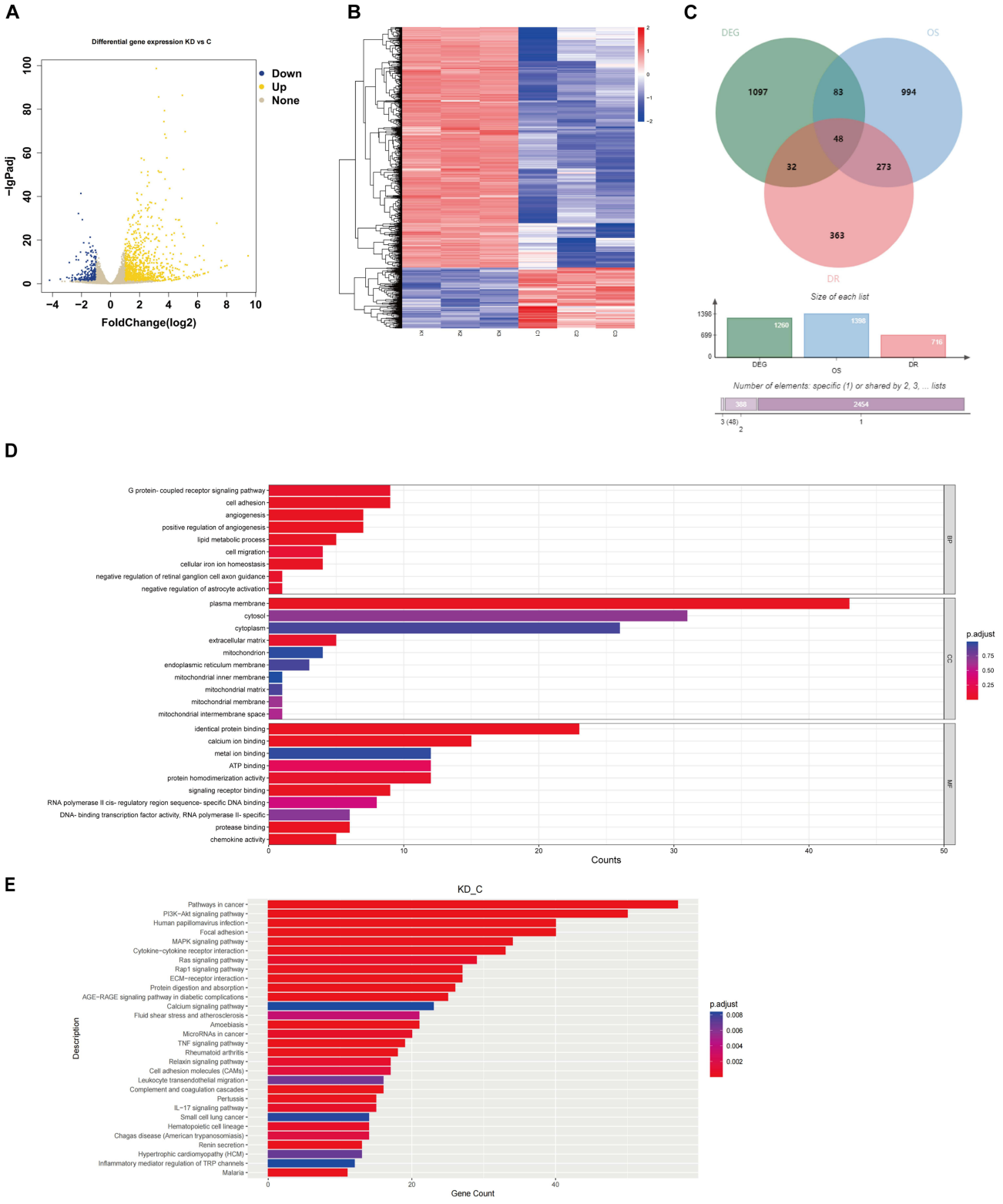

Figure 4 Knocking down TRAP1 affects oxidative stress and related mitochondrial functions in ARPE-19 cells. (**A**) Volcano plot of differentially expressed genes (DEGs) between shTRAP1 and NC, with yellow representing significantly upregulated genes and blue representing significantly downregulated genes (|log2 fold change|>1, log10 adjusted p-values<0.05). (**B**) Heatmap of DEGs between shTRAP1 and NC. (**C**) Venn diagram showing a high overlap between DEGs in the shTRAP1 group and oxidative stress-related genes (OS) and diabetic retinopathy-related risk genes (DR). (**D**) Gene Ontology (GO) enrichment analysis of DEGs. (**E**) Kyoto Encyclopedia of Genes and Genomes (KEGG) enrichment analysis of DEGs.

https://doi.org/10.2147/OPTH.S521660

exhibited a notable increase in mitochondrial membrane density with the disappearance of mitochondrial cristae (Figure 3J).

Concurrently, we investigated several well-known pathways of cell death. Following 3 days of HG stimulation in shTRAP1 cells, we introduced inhibitors targeting various cell death pathways, including Ferrostatin-1 (Fer-1), Z-VAD-FMK (Z-VAD), 3-Methyladenine (3-MA), and Necrostatin-1 (Nec-1). These inhibitors selectively address ferroptosis, apoptosis, autophagy, and necrosis pathways. After continued incubation for 3 days, the results indicated a substantial reduction in cell viability in the group without inhibitors, while the addition of Fer-1 markedly reversed the decline in cell viability (Figure 5A). These findings collectively underscore the important role of ferroptosis in HG-mediated cell death in shTRAP1 cells. Subsequently, we conducted a series of assessments related to ferroptosis. Analysis of cell viability demonstrated that the addition of the ferroptosis inducer Erastin to TRAP1^{OE}, shTRAP1, and control ARPE-19 cells under HG conditions revealed that TRAP1 upregulation conferred resistance to Erastin, whereas TRAP1 knockdown exacerbated the decrease in cell viability (Figure 5B). In the presence of Erastin, TRAP1^{OE} cells exhibited a reduction in MDA concentration compared to the control group, whereas shTRAP1 cells showed a significant increase in intracellular MDA concentration (Figure 5C). Moreover, the addition of Erastin resulted in a decrease in intracellular Fe^{2}+ concentration in TRAP1^{OE} cells compared to the control group, while shTRAP1 cells exhibited an elevated intracellular Fe^{2+} concentration (Figure 5D). Additionally, we assessed the intracellular ratio of reduced GSH to GSSG. This ratio reflects the redox state of the cell, and the addition of Erastin led to an increased ratio in TRAP1^{OE} cells compared to the control group, while shTRAP1 cells exhibited a significant decrease in the ratio (Figure 5E). Furthermore, we utilized C11 BODIPY 581/591 to measure lipid ROS levels. C11 BODIPY 581/591 is a ratio-type fluorescent probe that emits red fluorescence at 591nm when combined with normal cells. However, when cellular lipids undergo oxidation, the emission wavelength shifts from 591 nm to 510 nm, emitting green fluorescence. Consistently, TRAP1^{OE} cells showed a decrease in intracellular lipid ROS levels compared to the control group in the presence of Erastin, while shTRAP1 cells exhibited an increase in intracellular lipid ROS levels (Figure 5F). Under HG stimulation, ARPE-19 cell viability was impaired, and after 24h of treatment with Fer-1, cell viability was rescued, while the response of shTRAP1 cells to Fer-1 treatment was weaker (Figure 5G). On the other hand, in the presence of Fer-1, the MDA concentration in HG-stimulated shTRAP1 cells was higher than that in the control group (Figure 5H). Consistently, the Fe^{2+} concentration was also higher than that in the control group (Figure 5I). Furthermore, after the addition of Fer-1, the GSH/GSSG ratio in HG-stimulated shTRAP1 cells decreased compared to the control group (Figure 5J). When Fer-1 was added, intracellular lipid ROS levels in HG-stimulated shTRAP1 cells remained higher than that in the control group (Figure 5K).

To further explore the potential mechanisms by which TRAP1 alleviates hyperglycemia-induced ferroptosis, we performed co-immunoprecipitation (CO-IP) experiments on Control, TRAP1^{OE}, and TRAP1^{OE}+HG groups of ARPE19 cells to enrich TRAP1-binding proteins. Using mass spectrometry, we identified the types of proteins bound to TRAP1 and the differential proteins in these three groups of ARPE19 cells. Among them, we selected ACSL1, ACSL4, and CYB5R1 which closely related to ferroptosis and highly reliable in the mass spectrometry results—and verified them using Western blot analysis with the previously enriched proteins. We found an interaction between TRAP1 and ACSL1 in TRAP1^{OE}+HG group ARPE19 cells; an interaction between TRAP1 and ACSL4 in both TRAP1^{OE} and TRAP1^{OE}+HG groups; and an interaction between TRAP1 and CYB5R1 in both Control and TRAP1^{OE}+HG groups (Figure 5L).

In summary, our study suggests that TRAP1 may alleviate hyperglycemia-induced mitochondrial damage by inhibiting ferroptosis through its interaction with ACSL1, ACSL4, and CYB5R1, while the absence of TRAP1 exacerbates ferroptosis. This underscores the role of TRAP1 in enhancing cellular resistance to hyperglycemia-induced ferroptosis.

Discussion

DR is a progressive disease marked by early microaneurysms and retinal deposits advancing to neovascularization, tractional detachment, and blindness.[22] In DKD, TRAP1 similarly mitigates mitochondrial dysfunction by inhibiting mPTP opening through CypD interaction, reducing apoptosis and oxidative stress.[20] In DR, oxidative stress drives

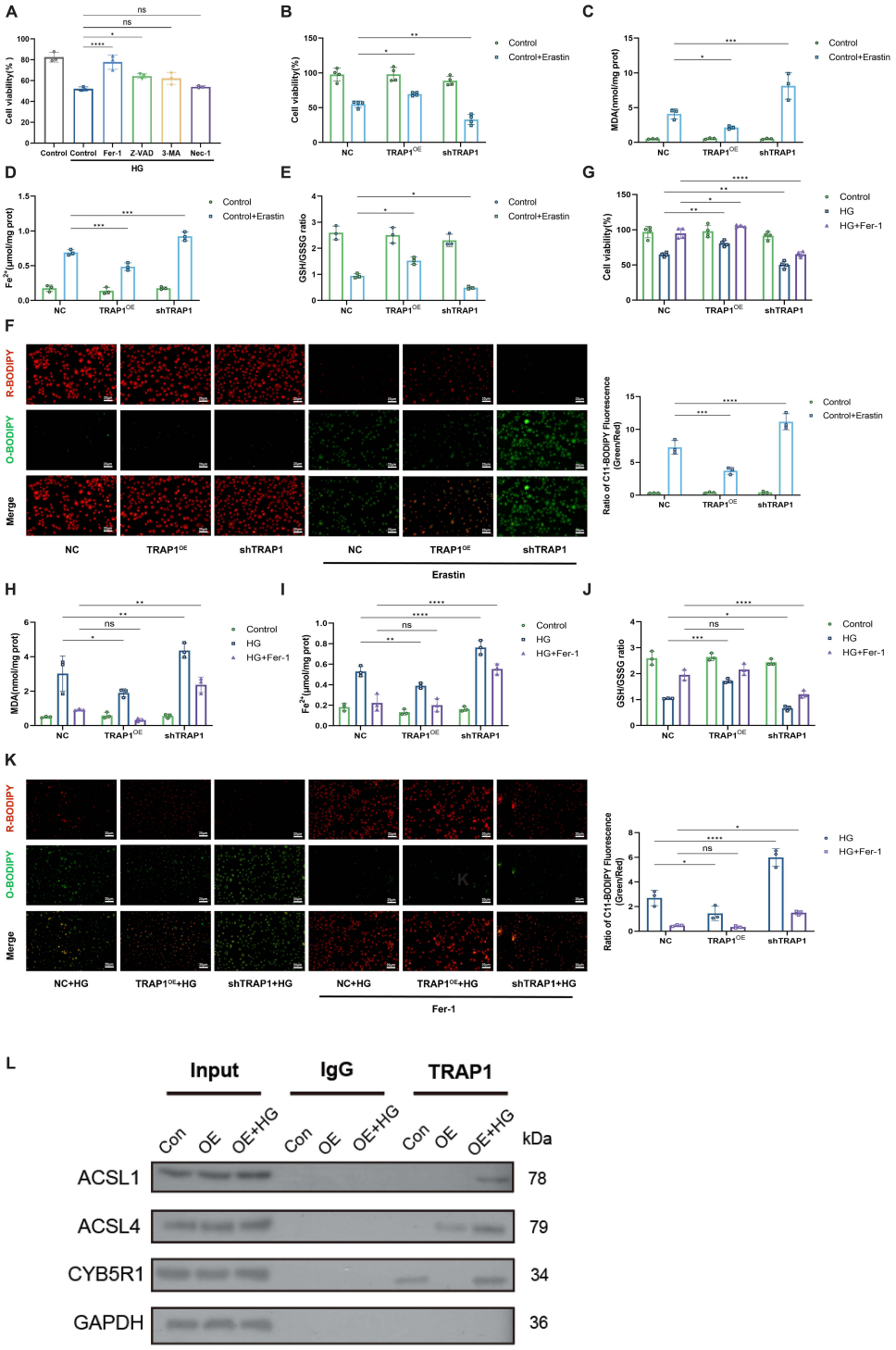

Figure 5 TRAP1 alleviates high glucose-induced cellular damage by inhibiting mitochondrial ferroptosis.(**A**) Activity of shTRAP1 cells treated with 50 mM glucose for 6 days or co-treated with Fer-1, Z-VAD, 3-MA, and Nec-1. (n=3) (**B**) Activity of NC, TRAP1^{OE}, and shTRAP1 cells treated with Erastin for 6 days or co-treated for 6 days. (n=4) (**C**) Intracellular MDA concentration of NC, TRAP1^{OE}, and shTRAP1 cells treated with Erastin for 6 days or co-treated for 6 days. (n=3) (**D**) Changes in intracellular Fe^{2+} concentration of NC, TRAP1^{OE}, and shTRAP1 cells treated with Erastin for 6 days or co-treated for 6 days. (n=3) (**E**) Ratio of GSH to GSSG in NC, TRAP1^{OE}, and shTRAP1 cells treated with Erastin for 6 days or co-treated for 6 days. (n=3) (**F**) Left panel: Fluorescence microscopy images showing the content of lipid ROS in NC, TRAP1^{OE}, and shTRAP1 cells treated with Erastin for 6 days or co-treated for 6 days. R-BODIPY: Reduced BODIPY(red). O-BODIPY: Oxidized BODIPY(green). Right panel: Quantitative data. Scale bar=20μm. (n=3) (**G**) Activity of NC, TRAP1^{OE}, and shTRAP1 cells treated with 50 mM glucose for 6 days or co-treated with Fer-1. (n=4) (**H**) Intracellular MDA concentration of NC, TRAP1^{OE}, and shTRAP1 cells treated with 50 mM glucose for 6 days or co-treated with Fer-1. (n=3) (**I**) Changes in intracellular Fe^{2+} concentration of NC, TRAP1^{OE}, and shTRAP1 cells treated with 50 mM glucose for 6 days or co-treated with Fer-1. (n=3) (**J**) Ratio of GSH to GSSG in NC, TRAP1^{OE}, and shTRAP1 cells treated with 50 mM glucose for 6 days or co-treated with Fer-1. (n=3) (**K**) Left panel: Fluorescence microscopy images showing the content of lipid ROS in NC, TRAP1^{OE}, and shTRAP1 cells treated with 50 mM glucose for 6 days or co-treated with Fer-1. Right panel: Quantitative data. Scale bar= 20μm. (n=3) (**L**) In Control, OE, and OE+HG groups of ARPE19 cells, immunoprecipitation (IP) was performed using TRAP1 antibody, and the enriched proteins were analyzed by Western Blot with antibodies against ACSL1, ACSL4, and CYB5R1. The error bars in the above histograms represent the mean±SD of independent experiments. ns P>0.05, *P<0.05, **P<0.01, ***P<0.001,****P<0.0001.

https://doi.org/10.2147/OPTH.S521660

mitochondrial ROS overproduction via ETC dysfunction, mtDNA damage, and AGE accumulation.[23–25] This initiates a vicious cycle of mPTP opening, CytC release, and further ROS generation.[26]

TRAP1 is one of the four subtypes of the HSP90 family, located in the inner mitochondrial membrane. It plays a important role in regulating metabolism and organelle homeostasis under stress conditions.[27] Studies have demonstrated that TRAP1 can directly inhibit succinate dehydrogenase (SDH) of the respiratory chain complex II, thereby downregulating OXPHOS and converting the respiratory activity of tumor cells into aerobic glycolysis, resulting in reduced mitochondrial ROS generation and protection of cellular redox homeostasis.[28–30]Tsai et al employed the HSP90 inhibitor Gamitrinib-TPP (G-TPP) in colon cancer cells and found that the inhibition of TRAP1 by G-TPP disrupted redox homeostasis, induced mitochondrial damage, and led to cell death.[31] Currently, TRAP1 is expressed in various cell types, with major studies involving brain, heart, and tumor cells.[32–34] Zhang et al demonstrated that in myocardial cells of diabetic patients, TRAP1 competes with the mitochondrial outer membrane protein MARCH5 for binding to the mitochondrial inner membrane protein MIC60, inhibiting MARCH5-mediated ubiquitination of MIC60, thus rescuing mitochondrial dysfunction and myocardial cell apoptosis under diabetic conditions.[35] Recent research has discovered TRAP1 expression in the mitochondria of human RPE cells. Silencing TRAP1 led to increased ROS production and impaired mitochondrial function in RPE cells, providing new insights into the treatment of age-related macular degeneration (AMD).[36] In this study, we found constitutive expression of TRAP1 in SD rat retinal layers, including Müller cells, ganglion cells, photoreceptor cells, and retinal pigment epithelial cells. However, TRAP1 expression decreased in STZ-induced diabetic rats, particularly in the RPE layer. This suggests pathological changes in TRAP1 under hyperglycemic stress conditions, which may be critically correlated with the occurrence and development of DR. Subsequently, we analyzed the downregulation of mitochondrial TRAP1 expression in ARPE-19 cells under sustained hyperglycemic stress, which is the first report in DR research. Interestingly, when exposed to 50mM glucose for 1–6 days, TRAP1 showed an initial increase followed by a decreasing trend. This may be due to the compensatory increase in TRAP1 as a heat shock protein under stress conditions, and when exposed to continuous high glucose for 2 days, the cell compensatory mechanism collapses, leading to a time-dependent decrease in TRAP1. Bhreathnach's study also confirmed a similar trend of upregulation followed by downregulation of TRAP1 expression in a mouse model of end-stage unilateral ureteral obstruction in diabetic nephropathy.[37]

Having demonstrated the downregulation of TRAP1 expression in RPE under high glucose conditions, we further investigated the protective role of TRAP1 on mitochondria. Overexpression of TRAP1 in ARPE-19 cells resulted in a significant reduction in cellular ROS generation and a notable increase in cell viability. Conversely, knocking down TRAP1 led to an increase in cellular ROS and enhanced cell death. Consistent with our findings, Zhang et al validated that TRAP1 downregulation exacerbates damage in H9C2 cells (rat myocardial cells) under high glucose conditions.[38] In the maintenance of mitochondrial homeostasis, the regulated opening of the mPTP plays a crucial role.[15] Mitochondria lacking CypD produce fewer swelling and permeability transitions, and CypD deficiency can protect neuronal cells from oxidative stress-induced cell death.[39] TRAP1 inhibits the opening of mPTP by directly interacting with CypD. MPTP opening leads to proton leakage, disruption of the mitochondrial inner and outer membrane potential, and a sharp decrease in $\Delta\psi m$.[40] Xiang et al studied neonatal rat primary cultured myocardial cells under hypoxic conditions and found that TRAP1 silencing reduced$\Delta\psi m$. Treatment with the mPTP inhibitor cyclosporin A rescued TRAP1 silencing-induced cell damage.[41] This phenomenon was also observed in NRK-52E cells under high glucose conditions and H9C cells exposed to extracellular acidification.[35,42] Our study confirmed that TRAP1 overexpression under high glucose stimulation increased $\Delta\psi m$ and reduced the extent of mPTP opening, while knocking down TRAP1 reversed this effect. The results suggest that TRAP1, as a heat shock protein, not only has physiological functions but also plays a crucial role in maintaining mitochondrial homeostasis and enhancing mitochondrial resistance to high glucose-induced damage.

Additionally, TEM revealed an increase in the number of mitochondria in ARPE-19 cells under high glucose stimulation, consistent with previous studies.[43] High glucose induces mitochondrial fission. Yu et al added Ad-DLP1-K38A to rat myocardial cells cultured under sustained high glucose conditions to block mitochondrial fission, and cellular ROS levels returned to normal.[44] Our TEM results showed that TRAP1 overexpression reduced the number of mitochondria in cells stimulated by HG, while TRAP1 knockdown significantly impaired cell status. This suggests that TRAP1 may inhibit mitochondrial fission, resulting in reduced ROS generation.

Based on previous research on TRAP1 and mitochondrial function, we conducted RNA-seq analysis on cells with TRAP1 knocked down under high glucose stimulation. The results indicated that differentially expressed genes overlapped with many oxidative stress-related genes and DR-related risk genes, suggesting that TRAP1 may play a crucial role in the occurrence and development of DR by regulating oxidative stress. Moreover, differentially expressed genes were significantly enriched in key biological processes such as cell adhesion, cell migration, inflammation, and angiogenesis, affecting mitochondrial protein complexes, mitochondrial matrix, and mitochondrial inner membrane functions, indicating the crucial role of TRAP1 in mitochondrial gene expression and protein function. The concept of ferroptosis, defined as a form of iron-dependent regulated cell death triggered by lipid peroxidation overload on the cell membrane, was first proposed by Dixon's team.[45] Many studies have confirmed that cellular ferroptosis plays a crucial role in diabetes and its complications.[46,47] Zhou et al found that the ROS scavenger N-acetylcysteine (NAC) inhibited ferroptosis in ARPE-19 cells cultured under high glucose conditions.[48] Recently, mitochondrial dysfunction has been found to induce ferroptosis, and mitochondria are considered the major organelles for iron-mediated oxidative damage. Thangal et al inhibited mitochondrial dysfunction using antioxidants such as NAC or a combination of mitochondrial antioxidants (SS31), anti-inflammatory drugs (amlexanox), and tranilast, finding a significant reduction in the occurrence of ferroptosis in ARPE-19 cells.[49] In our study, mitochondria in ARPE-19 cells under high glucose stimulation exhibited classical morphological features of ferroptosis, while cells overexpressing TRAP1 showed reduced membrane density and less pronounced cristae structure compared to the control group. TRAP1 knockdown resulted in a significant increase in mitochondrial membrane density, approaching the disappearance of cristae structures.

In our study, we observed that Fer-1 effectively rescued high glucose-induced cell death in the absence of TRAP1, indicating an enhanced involvement of the ferroptosis pathway in cells lacking TRAP1 under stress conditions, as compared to autophagy, apoptosis, and necrosis pathways. Consequently, a series of experiments were conducted to validate that TRAP1 overexpression significantly inhibits high glucose-induced ferroptosis in ARPE-19 cells, while TRAP1 deficiency markedly promotes ferroptosis under high glucose conditions. TRAP1 exerts its inhibitory role in cellular ferroptosis by attenuating ROS production within mitochondria and mitigating cellular oxidative stress. Previous research in clear cell renal cell carcinoma (ccRCC) has established a correlation between the SDH gene expression and ferroptosis genes, highlighting the role of SDH inhibition in reducing peroxide accumulation and suppressing cell ferroptosis.[50] Additionally, the voltage-dependent anion-selective channel 1 (VDAC1) is recognized as a critical target for iron-mediated cell death in acute liver injury induced by acetaminophen (APAP). APAP-induced VDAC1 oligomerization and mPTP opening exacerbate mitochondrial dysfunction and ferroptosis in liver cells. The application of the VDAC1 oligomerization inhibitor VBIT-12 significantly hinders liver cell ferroptosis.[51] Consistent with our findings,TRAP1 knockdown sustained mPTP opening, promoting cell ferroptosis, while TRAP1 overexpression inhibited mPTP opening, suppressing cell ferroptosis.

Despite our findings, our study has limitations. The effects of TRAP1 overexpression and knockdown were preliminarily explored in ARPE-19 cell models under high glucose conditions, but this cellular model may not entirely replicate the complex microenvironment in the diabetic patient's body. Further in vivo experiments are imperative to validate TRAP1 overexpression and knockdown models. Moreover, a deeper understanding of the molecular mechanisms through which TRAP1 inhibits cellular ferroptosis requires more comprehensive investigation.

Taken together, our research elucidates the protective role of TRAP1 in ARPE-19 cell mitochondria. Knocking down TRAP1 exacerbates mitochondrial damage, and the decline in TRAP1 levels may be a important factor in early DR mitochondrial dysfunction. Our findings affirm the correlation between TRAP1 and ferroptosis, underscoring TRAP1's capacity to enhance mitochondrial resistance against high glucose-induced damage, inhibit cellular ferroptosis, and improve cell viability. Targeting TRAP1 emerges as a promising therapeutic avenue for early DR, offering new prospects for DR treatment.

Conclusions

This study demonstrates that TRAP1 is constitutively expressed across retinal cell layers in STZ-induced DR rats, with its expression progressively declining as DR advances. In vitro, HGstimulation significantly reduced TRAP1 levels in

ARPE-19 cells, exacerbating mitochondrial dysfunction and diminishing cellular viability. Importantly, TRAP1 overexpression effectively preserved mitochondrial homeostasis under HG-induced stress, highlighting its critical role in counteracting metabolic perturbations. Furthermore, we established a novel link between TRAP1 and ferroptosis, revealing that TRAP1 enhances mitochondrial resilience to HG-induced oxidative damage, thereby suppressing ferroptosis and improving cell survival. The progressive decline in TRAP1 expression emerges as a pivotal contributor to mitochondrial dysfunction during the early stages of DR. Targeting TRAP1 to modulate mitochondrial integrity and ferroptosis pathways represents a promising therapeutic strategy for early DR intervention, offering potential clinical translation. Future studies should focus on validating these mechanisms in vivo and exploring TRAP1's broader role in diabetic complications.

Abbreviations

DR, Diabetes retinopathy; NPDR, Nonproliferative diabetes retinopathy; PDR, Proliferative diabetes retinopathy; ROS, Reactive oxygen species; AGEs, Advanced glycation end products; GSH, Glutathione; HSP90, Heat Shock Proteins 90; TRAP1, Tumor necrosis factor receptor-associated protein 1; ATP, Adenosine 5'-triphosphate; OXPHOS, Oxidative phosphorylation; NADPH, Nicotinamide adenine dinucleotide phosphate; mPTP, Mitochondrial permeability transition pore; VDAC1, Voltage-dependent anion channel 1; CypD, Cyclophilin D; CytC, Cytochrome complex; ETC, Electron transport chain; MIC60, Mitochondrial inner membrane protein 60; RPE, Retinal pigment epithelium; GPX4, Glutathione Peroxidase 4; CO-IP, Co-immunoprecipitation; ACSL1, Acyl-CoA synthetase long-chain family member 1; ACSL4, Acyl-CoA synthetase long-chain family member 4; CYB5R1, Cytochrome b5 reductase 1.

Data Sharing Statement

All data are included in the manuscript and supplementary material. The resources during the current study are available upon reasonable request.

Ethics Approval and Consent to Participate

All procedures conformed to the guidelines of the Association for Research and Vision and Ophthalmology statement for the use of animals in ophthalmic and vision research. This study was approved by the Ethics Committee of the First Affiliated Hospital of Nanjing Medical University, with the ethics number DWSY-22165292.

Acknowledgments

Yuchen Li, Weida Xu and Guiyang Zhao are co-first authors for this study. We would like to thank Bioinformatics for figure drawing.

This manuscript was submitted as a pre-print in the link "https://www.researchgate.net/publication/384576578_Trap1_Improves_Diabetic_Retinopathy_By_Preserving_Mitochondrial_Function.[52]

Author Contributions

All authors made a significant contribution to the work reported, whether that is in the conception, study design, execution, acquisition of data, analysis and interpretation, or in all these areas; took part in drafting, revising or critically reviewing the article; gave final approval of the version to be published; have agreed on the journal to which the article has been submitted; and agree to be accountable for all aspects of the work.

Funding

The study was supported in parts by grants from the Special Fund for Medical Science and Technology Development of Nanjing(YKK23112) and from National Natural Science Foundation of China(No.82000866).

Disclosure

The authors declare that they have no competing interests in this work.

References

1. Saeedi P, Petersohn I, Salpea P, et al. Global and regional diabetes prevalence estimates for 2019 and projections for 2030 and 2045: results from the international diabetes federation diabetes atlas. *Diabet Res Clin Pract*. 2019;157:107843. doi:10.1016/j.diabres.2019.107843
2. Kollias AN, Ulbig MW. Diabetic retinopathy: early diagnosis and effective treatment. *Dtsch Arztebl Int*. 2010;107(5):75–83. doi:10.3238/arztebl.2010.0075
3. Kang Q, Yang C. Oxidative stress and diabetic retinopathy: molecular mechanisms, pathogenetic role and therapeutic implications. *Redox Biol*. 2020;37:101799. doi:10.1016/j.redox.2020.101799
4. Alka K, Kumar J, Kowluru RA. Impaired mitochondrial dynamics and removal of the damaged mitochondria in diabetic retinopathy. *Front Endocrinol*. 2023;14:1160155. doi:10.3389/fendo.2023.1160155
5. Miller DJ, Cascio MA, Rosca MG. diabetic retinopathy: the role of mitochondria in the neural retina and microvascular disease. *Antioxidants*. 2020;9(10):905. doi:10.3390/antiox9100905
6. Zhang Q, Qu H, Chen Y, et al. Atorvastatin induces mitochondria-dependent ferroptosis via the modulation of Nrf2-xCT/GPx4 Axis. *Front Cell Dev Biol*. 2022;10:806081. doi:10.3389/fcell.2022.806081
7. Gao M, Yi J, Zhu J, et al. Role of mitochondria in ferroptosis. *Mol Cell*. 2019;73(2):354–63e3. doi:10.1016/j.molcel.2018.10.042
8. Krainz T, Gaschler MM, Lim C, Sacher JR, Stockwell BR, Wipf P. A mitochondrial-targeted nitroxide is a potent inhibitor of ferroptosis. *ACS Cent Sci*. 2016;2(9):653–659. doi:10.1021/acscentsci.6b00199
9. Masgras I, Laquatra C, Cannino G, Serapian SA, Colombo G, Rasola A. The molecular chaperone TRAP1 in cancer: from the basics of biology to pharmacological targeting. *Semin Cancer Biol*. 2021;76:45–53. doi:10.1016/j.semcancer.2021.07.002
10. Mayor A, Martinon F, De Smedt T, Petrilli V, Tschopp J. A crucial function of SGT1 and HSP90 in inflammasome activity links mammalian and plant innate immune responses. *Nat Immunol*. 2007;8(5):497–503. doi:10.1038/ni1459
11. Aguila M, Bevilacqua D, McCulley C, et al. Hsp90 inhibition protects against inherited retinal degeneration. *Hum Mol Genet*. 2014;23(8):2164–2175. doi:10.1093/hmg/ddt613
12. Dekker FA, Rudiger SGD. The mitochondrial hsp90 trap1 and alzheimer's disease. *Front Mol Biosci*. 2021;8:697913. doi:10.3389/fmolb.2021.697913
13. Ramos Rego I, Santos Cruz B, Ambrosio AF, Alves CH. TRAP1 in oxidative stress and neurodegeneration. *Antioxidants*. 2021;10(11):1829. doi:10.3390/antiox10111829
14. Lisanti S, Tavecchio M, Chae YC, et al. Deletion of the mitochondrial chaperone TRAP-1 uncovers global reprogramming of metabolic networks. *Cell Rep*. 2014;8(3):671–677. doi:10.1016/j.celrep.2014.06.061
15. Kang BH. TRAP1 regulation of mitochondrial life or death decision in cancer cells and mitochondria-targeted TRAP1 inhibitors. *BMB Rep*. 2012;45(1):1–6. doi:10.5483/BMBRep.2012.45.1.1
16. Montesano Gesualdi N, Chirico G, Pirozzi G, Costantino E, Landriscina M, Esposito F. Tumor necrosis factor-associated protein 1 (TRAP-1) protects cells from oxidative stress and apoptosis. *Stress*. 2007;10(4):342–350. doi:10.1080/10253890701314863
17. Matassa DS, Agliarulo I, Avolio R, Landriscina M, Esposito F. TRAP1 regulation of cancer metabolism: dual role as oncogene or tumor suppressor. *Genes*. 2018;9(4):195. doi:10.3390/genes9040195
18. Siegelin MD. Inhibition of the mitochondrial Hsp90 chaperone network: a novel, efficient treatment strategy for cancer? *Cancer Lett*. 2013;333(2):133–146. doi:10.1016/j.canlet.2013.01.045
19. Cannino G, Urbani A, Gaspari M, et al. The mitochondrial chaperone TRAP1 regulates F-ATP synthase channel formation. *Cell Death Differ*. 2022;29(12):2335–2346. doi:10.1038/s41418-022-01020-0
20. Liu L, Zhang L, Zhao J, et al. Tumor necrosis factor receptor-associated protein 1 protects against mitochondrial injury by preventing high glucose-induced mptp opening in diabetes. *Oxidative Med Cell Longev*. 2020;2020:6431517. doi:10.1155/2020/6431517
21. Chen Y, Schlotterer A, Kurowski L, et al. miRNA-124 prevents rat diabetic retinopathy by inhibiting the microglial inflammatory response. *IntJ Mol Sci*. 2023;24(3):2291. doi:10.3390/ijms24032291
22. Frank RN. Diabetic retinopathy. *N Engl J Med*. 2004;350(1):48–58. doi:10.1056/NEJMra021678
23. Kowluru RA, Kowluru A, Mishra M, Kumar B. Oxidative stress and epigenetic modifications in the pathogenesis of diabetic retinopathy. *Prog Retin Eye Res*. 2015;48:40–61. doi:10.1016/j.preteyeres.2015.05.001
24. Kowaltowski AJ, de Souza-Pinto NC, Castilho RF, Vercesi AE, de Souza-Pinto NC. Mitochondria and reactive oxygen species. *Free Radic Biol Med*. 2009;47(4):333–343. doi:10.1016/j.freeradbiomed.2009.05.004
25. Ying L, Shen Y, Zhang Y, et al. Association of advanced glycation end products with diabetic retinopathy in type 2 diabetes mellitus. *Diabet Res Clin Pract*. 2021;177:108880. doi:10.1016/j.diabres.2021.108880
26. Kent AC, El Baradie KBY, Hamrick MW. Targeting the mitochondrial permeability transition pore to prevent age-associated cell damage and neurodegeneration. *Oxid Med Cell Longev*. 2021;2021:6626484. doi:10.1155/2021/6626484
27. Erapian SA, Sanchez-Martin C, Moroni E, Rasola A, Colombo G. Targeting the mitochondrial chaperone TRAP1: strategies and therapeutic perspectives. *Trends Pharmacol Sci*. 2021;42(7):566–576. doi:10.1016/j.tips.2021.04.003
28. Chae YC, Caino MC, Lisanti S, et al. Control of tumor bioenergetics and survival stress signaling by mitochondrial HSP90s. *Cancer Cell*. 2012;22(3):331–344. doi:10.1016/j.ccr.2012.07.015
29. Rasola A, Neckers L, Picard D. Mitochondrial oxidative phosphorylation TRAP(1)ped in tumor cells. *Trends Cell Biol*. 2014;24(8):455–463. doi:10.1016/j.tcb.2014.03.005
30. Sciacovelli M, Guzzo G, Morello V, et al. The mitochondrial chaperone TRAP1 promotes neoplastic growth by inhibiting succinate dehydrogenase. *Cell Metab*. 2013;17(6):988–999. doi:10.1016/j.cmet.2013.04.019
31. Tsai HY, Bronner MP, March JK, et al. Metabolic targeting of NRF2 potentiates the efficacy of the TRAP1 inhibitor G-TPP through reduction of ROS detoxification in colorectal cancer. *Cancer Lett*. 2022;549:215915. doi:10.1016/j.canlet.2022.215915
32. Mitter SK, Song C, Qi X, et al. Dysregulated autophagy in the RPE is associated with increased susceptibility to oxidative stress and AMD. *Autophagy*. 2014;10(11):1989–2005. doi:10.4161/auto.36184
33. Barbosa IA, Vega-Naredo I, Loureiro R, et al. TRAP1 regulates autophagy in lung cancer cells. *Eur J Clin Invest*. 2018;48(4). doi:10.1111/eci.12900.

34. Quinn PM, Buck TM, Ohonin C, Mikkers HMM, Wijnholds J. Production of iPS-derived human retinal organoids for use in transgene expression assays. *Methods Mol Biol*. 2018;1715:261–273.
35. Zhang L, Luo Y, Lv L, Chen S, Liu G, Zhao T. TRAP1 inhibits MARCH5-mediated MIC60 degradation to alleviate mitochondrial dysfunction and apoptosis of cardiomyocytes under diabetic conditions. *Cell Death Differ*. 2023;30(10):2336–2350. doi:10.1038/s41418-023-01218-w
36. Ramos Rego I, Silvério D, Eufrásio MI, et al. TRAP1 is expressed in human retinal pigment epithelial cells and is required to maintain their energetic status. *Antioxidants*. 2023;12(2):381. doi:10.3390/antiox12020381
37. Bhreathnach U, Griffin B, Brennan E, Ewart L, Higgins D, Murphy M. Profibrotic IHG-1 complexes with renal disease associated HSPA5 and TRAP1 in mitochondria. *Biochim Biophys Acta Mol Basis Dis*. 2017;1863(4):896–906. doi:10.1016/j.bbadis.2017.01.015
38. Zhang X, Zhong Z, Li W. Downregulation of TRAP1 aggravates injury of H9c2 cardiomyocytes in a hyperglycemic state. *Exp Ther Med*. 2019;18 (4):2681–2686. doi:10.3892/etm.2019.7847
39. Laquatra C, Sanchez-Martin C, Dinarello A, et al. HIF1alpha-dependent induction of the mitochondrial chaperone TRAP1 regulates bioenergetic adaptations to hypoxia. *Cell Death Dis*. 2021;12(5):434. doi:10.1038/s41419-021-03716-6
40. Yang KM, Pyo JO, Kim GY, et al. Capsaicin induces apoptosis by generating reactive oxygen species and disrupting mitochondrial transmembrane potential in human colon cancer cell lines. *Cell Mol Biol Lett*. 2009;14(3):497–510. doi:10.2478/s11658-009-0016-2
41. Xiang F, Huang YS, Shi XH, Zhang Q. Mitochondrial chaperone tumour necrosis factor receptor-associated protein 1 protects cardiomyocytes from hypoxic injury by regulating mitochondrial permeability transition pore opening. *FEBS J*. 2010;277(8):1929–1938. doi:10.1111/j.1742-4658.2010.07615.x
42. Zhang L, Liu L, Li X, et al. TRAP1 attenuates H9C2 myocardial cell injury induced by extracellular acidification via the inhibition of MPTP opening. *Int J Mol Med*. 2020;46(2):663–674. doi:10.3892/ijmm.2020.4631
43. Sun Y, Ge X, Li X, et al. High-fat diet promotes renal injury by inducing oxidative stress and mitochondrial dysfunction. *Cell Death Dis*. 2020;11 (10):914. doi:10.1038/s41419-020-03122-4
44. Yu T, Sheu SS, Robotham JL, Yoon Y. Mitochondrial fission mediates high glucose-induced cell death through elevated production of reactive oxygen species. *Cardiovasc Res*. 2008;79(2):341–351. doi:10.1093/cvr/cvn104
45. Dixon SJ, Lemberg KM, Lamprecht MR, et al. Ferroptosis: an iron-dependent form of nonapoptotic cell death. *Cell*. 2012;149(5):1060–1072. doi:10.1016/j.cell.2012.03.042
46. Wang X, Chen X, Zhou W, et al. Ferroptosis is essential for diabetic cardiomyopathy and is prevented by sulforaphane via AMPK/NRF2 pathways. *Acta Pharm Sin B*. 2022;12(2):708–722. doi:10.1016/j.apsb.2021.10.005
47. Kim S, Kang SW, Joo J, et al. Characterization of ferroptosis in kidney tubular cell death under diabetic conditions. *Cell Death Dis*. 2021;12 (2):160. doi:10.1038/s41419-021-03452-x
48. Zhou J, Sun C, Dong X, Wang H. A novel miR-338-3p/SLC1A5 axis reprograms retinal pigment epithelium to increases its resistance to high glucose-induced cell ferroptosis. *J Mol Histol*. 2022;53(3):561–571. doi:10.1007/s10735-022-10070-0
49. Yumnamcha T, Devi TS, Singh LP. Auranofin mediates mitochondrial dysregulation and inflammatory cell death in human retinal pigment epithelial cells: implications of retinal neurodegenerative diseases. *Front Neurosci*. 2019;13:1065. doi:10.3389/fnins.2019.01065
50. Yang J, Zhou Y, Li Y, et al. Functional deficiency of succinate dehydrogenase promotes tumorigenesis and development of clear cell renal cell carcinoma through weakening of ferroptosis. *Bioengineered*. 2022;13(4):11187–11207. doi:10.1080/21655979.2022.2062537
51. Niu B, Lei X, Xu Q, et al. Protecting mitochondria via inhibiting VDAC1 oligomerization alleviates ferroptosis in Acetaminophen-induced acute liver injury. *Cell Biol Toxicol*. 2022;38(3):505–530. doi:10.1007/s10565-021-09624-x
52. Yuchen L, Weida X, Zhao G, et al. Trap1 improves diabetic retinopathy by preserving mitochondrial function. doi:10.2139/ssrn.4963593